
Learning Graph Structure from Convolutional Mixtures

Max Wasserman

Dept. of Computer Science
University of Rochester
Rochester, NY 14627
mwasser6@cs.rochester.edu

Saurabh Sihag

Dept. of Electrical and Systems Eng.
University of Pennsylvania
Philadelphia, PA 19104
sihags@pennmedicine.upenn.edu

Gonzalo Mateos

Dept. of Electrical and Computer Eng.
University of Rochester
Rochester, NY 14620
gmateos@ece.rochester.edu

Alejandro Ribeiro

Dept. of Electrical and Systems Eng.
University of Pennsylvania
Philadelphia, PA 19104
aribeiro@seas.upenn.edu

Abstract

Machine learning frameworks such as graph neural networks typically rely on a given, fixed graph to exploit relational inductive biases and thus effectively learn from network data. However, when said graphs are (partially) unobserved, noisy, or dynamic, the problem of inferring graph structure from data becomes relevant. In this paper, we postulate a graph convolutional relationship between the observed and latent graphs, and formulate the graph learning task as a network inverse (deconvolution) problem. In lieu of eigendecomposition-based spectral methods or iterative optimization solutions, we unroll and truncate proximal gradient iterations to arrive at a parameterized neural network architecture that we call a Graph Deconvolution Network (GDN). GDNs can learn a distribution of graphs in a supervised fashion, perform link prediction or edge-weight regression tasks by adapting the loss function, and they are inherently inductive. We corroborate GDN's superior graph recovery performance and its generalization to larger graphs using synthetic data in supervised settings. Furthermore, we demonstrate the robustness and representation power of GDNs on real world neuroimaging and social network datasets.

1 Introduction

Inferring graphs from data to uncover latent complex information structure is a timely challenge for geometric deep learning [1] and graph signal processing (GSP) [2]. But it is also an opportunity, since network topology inference advances [3, 4, 5] could facilitate adoption of graph neural networks (GNNs) even when no input graph is available [6]. The problem is also relevant when a given graph is too noisy or perturbed beyond what stable (possibly pre-trained) GNN architectures can effectively handle [7]. Early empirical evidence suggests that even when a graph is available, the structure could be further optimized for a downstream task [8, 9], or else sparsified to boost computational efficiency and model interpretability [10].

In this paper, we posit a convolutional model relating observed and latent undirected graphs and formulate the graph learning task as a supervised network inverse problem; see Section 2 for a formal problem statement. This fairly general model is motivated by various practical domains outlined in Section 3, such as identifying the structure of network diffusion processes [11, 12], as well as

network deconvolution and denoising [8]. We propose a parameterized neural network (NN) model, termed graph deconvolution network (GDN), which we train in a supervised fashion to learn the distribution of latent graphs. The architecture is derived from the principle of algorithm unrolling used to learn fast approximate solutions to inverse problems [13, 14, 15], an idea that is yet to be fully explored for graph structure identification. Since layers directly operate on, combine, and refine graph objects (instead of nodal features), GDNs are inherently inductive and can generalize to graphs of different size. This allows the transfer of learning on small graphs to unseen larger graphs, which has significant implications in domains like social networks and molecular biology [16]. Our experiments demonstrate that GDNs are versatile to accommodate link prediction or edge-weight regression aspects of learning the graph structure, and achieve superior performance over various competing alternatives. Building on recent models of functional activity in the brain as a diffusion process over the underlying anatomical pathways [17, 18], we show the applicability of GDNs to infer brain structural connectivity from functional networks obtained from the Human Connectome Project-Young Adult (HCP-YA) dataset. We also use GDNs to predict Facebook ties from user co-location data, outperforming relevant baselines.

Related Work. Network topology inference has a long history in statistics [19], with noteworthy contributions for probabilistic graphical model selection; see e.g. [20, 21, 22]. Recent advances were propelled by GSP insights through the lens of signal representation [3, 4, 5], exploiting models of network diffusion [23], or else leveraging cardinal properties of network data such as smoothness [24, 25] and graph stationarity [11, 12]. These works formulate (convex) optimization problems one has to solve for different graphs, and can lack robustness to signal model misspecifications. Scalability is an issue for the spectral-based network deconvolution approaches in [11, 8], that require computationally-expensive eigendecompositions of the input graph for each problem instance. Moreover, none of these methods advocate a supervised learning paradigm to learn distributions over adjacency matrices. When it comes to this latter objective, deep generative models [26, 27, 28] are typically trained in an unsupervised fashion, with the different goal of sampling from the learnt distribution. Most of these approaches learn node embeddings and are inherently transductive. Recently, so-termed latent graph learning has been shown effective in obtaining better task-driven representations of relational data for machine learning (ML) applications [29, 9, 30], or to learn interactions among coupled dynamical systems [31]. Algorithm unrolling has only recently been adopted for graph learning in [32, 33], for different and more specific problems subsumed by the network deconvolution framework dealt with here. Indeed, [32] focuses on Gaussian graphical model selection in a supervised learning setting and [33] learns graph topologies under a smoothness signal prior.

Summary of contributions. We introduce GDNs, a supervised learning model capable of recovering latent graph structure from observations of its convolutional mixtures, i.e., related graphs containing spurious, indirect relationships. Our experiments on synthetic and real datasets demonstrate the effectiveness of GDNs for said task. They also showcase the model’s versatility to incorporate domain-specific topology information about the sought graphs. On synthetic data, GDNs outperform comparable methods on link prediction and edge-weight regression tasks across different random-graph ensembles, while incurring a markedly lower (post-training) computational cost and inference time. GDNs are inductive and learnt models transfer across graphs of different sizes. We verify they exhibit minimal performance degradation even when tested on graphs $30\times$ larger. GDNs are used to learn Facebook friendships from mobility data, effectively deconvolving spurious relations from measured co-location interactions among high school students. Finally, using GDNs we propose a novel ML pipeline to learn whole brain structural connectivity (SC) from functional connectivity (FC), a challenging and timely problem in network neuroscience. Results on the high-quality HCP-YA imaging dataset show that GDNs perform well on specific brain subnetworks that are known to be relatively less correlated with the corresponding FC due to ageing-related effects – a testament to the model’s robustness and expressive power. Overall, results here support the promising prospect of using graph representation learning to integrate brain structure and function.

2 Problem Formulation

In this work we study the following network inverse problem involving undirected and weighted graphs $\mathcal{G}(\mathcal{V}, \mathcal{E})$, where $\mathcal{V} = \{1, \dots, N\}$ is the set of nodes (henceforth common to all graphs), and $\mathcal{E} \subseteq \mathcal{V} \times \mathcal{V}$ collects the edges. We get to observe a graph with symmetric adjacency matrix

$\mathbf{A}_O \in \mathbb{R}^{N \times N}$, that is related to a latent sparse, graph $\mathbf{A}_L \in \mathbb{R}_+^{N \times N}$ of interest via the data model

$$\mathbf{A}_O = h_0 \mathbf{I} + h_1 \mathbf{A}_L + \dots + h_K \mathbf{A}_L^K \quad (1)$$

for some $K \leq N - 1$ by the Cayley-Hamilton theorem. Matrix polynomials $\mathbf{H}(\mathbf{A}; \mathbf{h}) := \sum_{k=0}^K h_k \mathbf{A}^k$ with coefficients $\mathbf{h} := [h_0, \dots, h_K]^\top \in \mathbb{R}^{K+1}$, are known as shift-invariant graph convolutional filters; see e.g., [2, 34]. We postulate that $\mathbf{A}_O = \mathbf{H}(\mathbf{A}_L; \mathbf{h})$ for some filter order K and its associated coefficients \mathbf{h} , such that we can think of the observed network as generated via a graph convolutional process acting on \mathbf{A}_L . That is, one can think of \mathbf{A}_O as a graph containing spurious, indirect connections generated by the higher-order terms in the latent graph \mathbf{A}_L – the graph of fundamental relationships. More pragmatically \mathbf{A}_O may correspond to a noisy observation of $\mathbf{H}(\mathbf{A}_L; \mathbf{h})$, and this will be clear from the context when e.g., we estimate \mathbf{A}_O from data.

Recovery of the latent graph \mathbf{A}_L is a challenging endeavour since we do not know $\mathbf{H}(\mathbf{A}_L; \mathbf{h})$, namely the parameters K or \mathbf{h} ; see Appendix A.1 for issues of model identifiability and their relevance to the problem dealt with here. Suppose that \mathbf{A}_L is drawn from some distribution of sparse graphs, e.g., random geometric graphs or structural brain networks from a homogeneous dataset. Then given independent training samples $\mathcal{T} := \{\mathbf{A}_O^{(i)}, \mathbf{A}_L^{(i)}\}_{i=1}^T$ adhering to (1), our goal is to learn a parametric mapping Φ that predicts the graph adjacency matrix $\hat{\mathbf{A}}_L = \Phi(\mathbf{A}_O; \Theta)$ by minimizing a loss function

$$L(\Theta) := \frac{1}{T} \sum_{i \in \mathcal{T}} \ell(\mathbf{A}_L^{(i)}, \Phi(\mathbf{A}_O^{(i)}; \Theta)) \quad (2)$$

to search for the best parameters Θ . The loss ℓ is adapted to the task at hand – hinge loss for link prediction or mean-squared error for the more challenging edge-weight regression problem; see Appendix A.4. Notice that (1) postulates a common filter across graph pairs in \mathcal{T} – a simplifying assumption shown to be tenable in fMRI studies [17] where subject-level filters exhibit limited variability. This will be relaxed when we customize the GDN architecture; see Section 4.3 for details.

3 Motivating Application Domains and the Supervised Setting

Here we outline several graph inference tasks that can be cast as the network inverse problem (1), and give numerous examples supporting the relevance of the novel supervised setting.

Graph structure identification from diffused signals. Our initial focus is on identifying graphs that explain the structure of a class of network diffusion processes. Formally, let $\mathbf{x} \in \mathbb{R}^N$ be a graph signal (i.e., a vector of nodal features) supported on a latent graph \mathcal{G} with adjacency \mathbf{A}_L . Further, let \mathbf{w} be a zero-mean white signal with covariance matrix $\Sigma_w = \mathbb{E}[\mathbf{w}\mathbf{w}^\top] = \mathbf{I}$. We say that \mathbf{A}_L represents the structure of the signal \mathbf{x} if there exists a linear network diffusion process in \mathcal{G} that generates the signal \mathbf{x} from \mathbf{w} , namely $\mathbf{x} = \sum_{i=0}^{\infty} \alpha_i \mathbf{A}_L^i \mathbf{w} = \mathbf{H}(\mathbf{A}_L; \mathbf{h})\mathbf{w}$. This is a fairly common generative model for random network processes [35, 36]. We think of the edges of \mathcal{G} as direct (one-hop) relations between the elements of the signal \mathbf{x} . The diffusion described by $\mathbf{H}(\mathbf{A}_L; \mathbf{h})$ generates indirect relations. In this context, the latent graph learning problem is to recover a sparse \mathbf{A}_L from a set $\mathcal{X} := \{\mathbf{x}_i\}_{i=1}^P$ of P samples of \mathbf{x} [11]. Interestingly, from the model for \mathbf{x} it follows that the signal covariance matrix $\Sigma_x = \mathbb{E}[\mathbf{x}\mathbf{x}^\top] = \mathbf{H}(\mathbf{A}_L; \mathbf{h})^2$ is also a polynomial in \mathbf{A}_L – precisely the relationship prescribed by (1) when identifying $\mathbf{A}_O = \Sigma_x$. In practice, given the signals in \mathcal{X} one would estimate the covariance matrix, e.g. via the sample covariance $\hat{\Sigma}_x$, and then aim to recover the graph \mathbf{A}_L by tackling the aforementioned network inverse problem. In this paper, we propose a fresh learning-based solution using training examples $\mathcal{T} := \{\hat{\Sigma}_x^{(i)}, \mathbf{A}_L^{(i)}\}_{i=1}^T$.

Network deconvolution and denoising. The network deconvolution problem is to identify a sparse adjacency matrix \mathbf{A}_L that encodes direct dependencies, when given an adjacency matrix \mathbf{A}_O containing extraneous indirect relationships. The problem broadens the scope of signal deconvolution to networks and can be tackled by attempting to invert the mapping $\mathbf{A}_O = \mathbf{A}_L (\mathbf{I} - \mathbf{A}_L)^{-1} = \sum_{i=1}^{\infty} \mathbf{A}_L^i$. This solution proposed in [8] assumes a polynomial relationship as in (1), but for the particular case of a single-pole, single-zero graph filter with very specific filter coefficients [cf. (1) with $\alpha_0 = 0$ and $\alpha_i = 1, i \geq 1$]. This way, the indirect dependencies observed in \mathbf{A}_O arise due to the higher-order convolutive mixture terms $\mathbf{A}_L^2 + \mathbf{A}_L^3 + \dots$ superimposed to the direct interactions in \mathbf{A}_L we wish to recover. We adopt a data-driven learning approach in assuming that \mathbf{A}_O can be written as a polynomial in \mathbf{A}_L , but being agnostic to the form of the filter, thus generalizing the problem

setting. Unlike the problem outlined before, here \mathbf{A}_O need not be a covariance matrix. Indeed, \mathbf{A}_O could be a corrupted graph we wish to denoise, obtained via an upstream graph learning method. Potential application domains for which supervised data $\mathcal{T} := \{\mathbf{A}_O^{(i)}, \mathbf{A}_L^{(i)}\}_{i=1}^T$ is available include bioinformatics (infer protein contact structure from mutual information graphs of the covariation of amino acid residues [8]), gene regulatory network inference from microarray data (see e.g. the DREAM5 project to reconstruct networks for the E. coli bacterium and single-cell eukaryotes), social and information networks (e.g., learn to sparsify graphs [10] to unveil the most relevant collaborations in a social network encoding co-authorship information [11]), and epidemiology (such as contact tracing by deconvolving the graphs that model observed disease spread in a population). In Section 5.2 we experiment with social networks and the network neuroscience problem described next.

Inferring structural brain networks from functional MRI (fMRI) signals. Brain connectomes encompass networks of brain regions connected by (statistical) functional associations (FC) or by anatomical white matter fiber pathways (SC). The latter can be extracted from time-consuming tractography algorithms applied to diffusion MRI (dMRI), which are particularly fraught due to quality issues in the data [37]. FC represents pairwise correlation structure between blood-oxygen-level-dependent (BOLD) signals measured by fMRI. Deciphering the relationship between SC and FC is a very active area of research [17, 38] and also relevant in studying neurological disorders, since it is known to vary with respect to healthy subjects in pathological contexts [39]. Traditional approaches go all the way from correlation studies [40] to large-scale simulations of nonlinear cortical activity models [38]. More aligned with the problem addressed here, recent studies have shown that linear diffusion dynamics can reasonably model the FC-SC coupling [17]. Using our notation, the findings in [17] suggest that the covariance $\mathbf{A}_O = \Sigma_x$ of the functional signals (i.e., the FC) is related to the the sparse SC graph \mathbf{A}_L via the model in (1). Similarly, [18] contend FC can be modeled as a weighted sum of powers of the SC matrix, consisting of both direct and indirect effects along varying paths. There is evidence that FC links tend to exist where there is no or little structural connection [41], a property naturally captured by (1). These considerations motivate adopting our graph learning method to infer SC patterns from fMRI signals using the training set $\mathcal{T} := \{\mathbf{FC}^{(i)}, \mathbf{SC}^{(i)}\}_{i=1}^T$ (Section 5.2), a significant problem for several reasons. The ability to collect only FC and get informative estimates of SC open the door to large scale studies, previously constrained by the logistical, cost, and computational resources needed to acquire both modalities.

4 Graph Deconvolution Network

Here we present the proposed GDN model, a NN architecture that we train in a supervised fashion to recover latent graph structure. In the sequel, we obtain ‘conceptual’ iterations to tackle an optimization formulation of the network inverse problem (Section 4.1), unroll these iterations to arrive at the parametric, differentiable GDN function $\Phi(\mathbf{A}_O; \Theta)$ we train using graph data \mathcal{T} (Section 4.2), and describe architectural customizations to improve performance (Section 4.3).

4.1 Motivation via iterative optimization

Going back to the inverse problem of recovering a sparse adjacency matrix \mathbf{A}_L from the mixture \mathbf{A}_O in (1), if the graph filter $\mathbf{H}(\mathbf{A}; \mathbf{h})$ were known – but recall it is not – we could attempt to solve

$$\hat{\mathbf{A}}_L \in \arg \min_{\mathbf{A} \in \mathcal{A}} \left\{ \|\mathbf{A}\|_1 + \frac{\lambda}{2} \|\mathbf{A}_O - \mathbf{H}(\mathbf{A}; \mathbf{h})\|_F^2 \right\}, \quad (3)$$

where $\lambda > 0$ trades off sparsity for reconstruction error. The convex set $\mathcal{A} := \{\mathbf{A} \in \mathbb{R}^{N \times N} \mid \text{diag}(\mathbf{A}) = \mathbf{0}, A_{ij} = A_{ji} \geq 0, \forall i, j \in \{1, \dots, N\}\}$ encodes the admissibility constraints on the adjacency matrix of an undirected graph: hollow diagonal, symmetric, with non-negative edge weights. The ℓ_1 norm encourages sparsity in the solution, being a convex surrogate of the edge-cardinality function that counts the number of non-zero entries in \mathbf{A} . Since \mathbf{A}_O is often a noisy observation or estimate of the polynomial $\mathbf{H}(\mathbf{A}_L; \mathbf{h})$, it is prudent to relax the equality (1) and minimize the squared residual errors instead.

The composite cost in (3) is a weighted sum of a non-smooth function $\|\mathbf{A}\|_1$ and a continuously differentiable function $g(\mathbf{A}) := \frac{1}{2} \|\mathbf{A}_O - \mathbf{H}(\mathbf{A}; \mathbf{h})\|_F^2$. Notice though that $g(\mathbf{A})$ is non-convex and its gradient is only locally Lipschitz continuous due to the graph filter $\mathbf{H}(\mathbf{A}; \mathbf{h})$; except when $K = 1$, but the affine case is not interesting since \mathbf{A}_O is just a scaled version of \mathbf{A}_L . Leveraging the

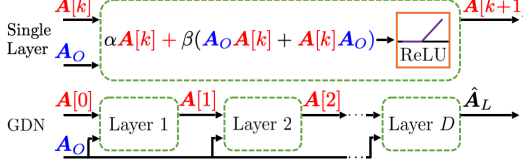


Figure 1: Schematic of GDN architecture.

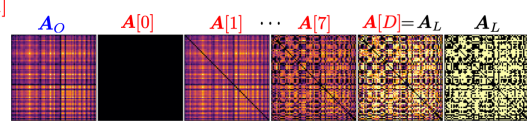


Figure 2: GDN intermediate layer outputs.

polynomial structure of the non-convexity, provably convergent iterations can be derived using e.g., the Bregman proximal gradient method [42] for judiciously chosen kernel generating distance; see also [43]. But our end goal here is not to solve (3) iteratively, recall we cannot even formulate the problem because $\mathbf{H}(\mathbf{A}; \mathbf{h})$ is unknown. To retain the essence of the problem structure and motivate a parametric model to learn approximate solutions, it suffices to settle with ‘conceptual’ proximal gradient (PG) iterations (k henceforth denote iterations, $\mathbf{A}[0] \in \mathcal{A}$)

$$\mathbf{A}[k+1] = \text{ReLU}(\mathbf{A}[k] - \tau \nabla g(\mathbf{A}[k]) - \tau \mathbf{1}\mathbf{1}^\top) \quad (4)$$

for $k = 0, 1, 2, \dots$, where τ is a step-size parameter in which we have absorbed λ . These iterations implement a gradient descent step on g followed by the ℓ_1 norm’s proximal operator; for more on PG algorithms see [44]. Due to the non-negativity constraints in \mathcal{A} , the ℓ_1 norm’s proximal operator takes the form of a τ -shifted ReLU on the off-diagonal entries of its matrix argument. Also, the operator sets $\text{diag}(\mathbf{A}[k+1]) = \mathbf{0}$. We cannot run (4) without knowledge of \mathbf{h} , and we will make no attempt to estimate \mathbf{h} . Instead, we unroll and truncate these iterations (and in the process, convert unknowns to learnable parameters Θ) to arrive at the trainable GDN parametric model $\Phi(\mathbf{A}_O; \Theta)$.

4.2 Learning to infer graphs via algorithm unrolling

The idea of algorithm unrolling can be traced back to the seminal work of [13]. In the context of sparse coding, they advocated identifying *iterations* of PG algorithms with *layers* in a deep network of fixed depth that can be trained from examples using backpropagation. One can view this process as effectively truncating the iterations of an asymptotically convergent procedure, to yield a template architecture that learns to approximate solutions with substantial computational savings relative to the optimization algorithm. Beyond parsimonious signal modeling, there has been a surge in popularity of unrolled deep networks for a wide variety of applications; see e.g., [15] for a recent tutorial treatment focused on signal and image processing. However, to the best of our knowledge this approach is yet to be fully explored for latent graph learning; see [32, 33] for recent inspiring attempts that can face scalability issues when operating on large graphs. A detailed account of the differences between GDN and the GLAD approach in [32] is given in Appendix A.8.

Building on the algorithm unrolling paradigm, we design a non-linear, parameterized, feed-forward architecture that can be trained to predict the latent graph $\hat{\mathbf{A}}_L = \Phi(\mathbf{A}_O; \Theta)$. To this end, we approximate the gradient $\nabla g(\mathbf{A})$ by retaining only linear terms in \mathbf{A} , and build a deep network by composing layer-wise linear filters and point-wise nonlinearities to capture higher-order interactions in the generative process $\mathbf{H}(\mathbf{A}; \mathbf{h}) := \sum_{k=0}^K h_k \mathbf{A}^k$. In more detail, we start by simplifying $\nabla g(\mathbf{A})$ (derived in Appendix A.6) by dropping all higher-order terms in \mathbf{A} , namely

$$\begin{aligned} \nabla g(\mathbf{A}) &= - \sum_{k=1}^K h_k \sum_{r=0}^{k-1} \mathbf{A}^{k-r-1} \mathbf{A}_O \mathbf{A}^r + \frac{1}{2} \nabla_{\mathbf{A}} \text{Tr} [\mathbf{H}^2(\mathbf{A}; \mathbf{h})] \\ &\approx -h_1 \mathbf{A}_O - h_2 (\mathbf{A}_O \mathbf{A} + \mathbf{A} \mathbf{A}_O) + (2h_0 h_2 + h_1^2) \mathbf{A}. \end{aligned} \quad (5)$$

Notice that $\nabla_{\mathbf{A}} \text{Tr} [\mathbf{H}^2(\mathbf{A}; \mathbf{h})]$ is a polynomial of degree $2K - 1$. Hence, we keep the linear term in \mathbf{A} but drop the constant offset that is proportional to \mathbf{I} , which is inconsequential to adjacency matrix updates with null diagonal. An affine approximation will lead to more benign optimization landscapes when it comes to training the resulting GDN model; see section 5 for ablation studies exploring the effects of higher-order terms in the approximation. All in all, the PG iterations become

$$\mathbf{A}[k+1] = \text{ReLU}(\alpha \mathbf{A}[k] + \beta (\mathbf{A}_O \mathbf{A}[k] + \mathbf{A}[k] \mathbf{A}_O) + \gamma \mathbf{A}_O - \tau \mathbf{1}\mathbf{1}^\top), \quad (6)$$

where $\mathbf{A}[0] \in \mathcal{A}$ and we defined $\alpha := (1 - 2\tau h_0 h_2 - \tau h_1^2)$, $\beta := \tau h_2$, and $\gamma := \tau h_1$. The latter parameter triplet encapsulates filter (i.e., mixture) coefficients and the λ -dependent algorithm step-size, all of which are unknown in practice.

The GDN architecture is thus obtained by unrolling the iterations (6) into a deep NN; see Figure 1. This entails mapping each individual iteration into a layer and stacking a prescribed number D of layers together to form $\Phi(\mathbf{A}_O; \Theta)$. The unknown filter coefficients are treated as learnable parameters $\Theta := \{\alpha, \beta, \gamma, \tau\}$, which are shared across layers as in recurrent neural networks (RNNs). The reduced number of parameters relative to most typical NNs is a characteristic of unrolled networks [15]. In the next section, we will explore a few customizations to the architecture in order to broaden the model’s expressive power. Given a training set $\mathcal{T} = \{\mathbf{A}_O^{(i)}, \mathbf{A}_L^{(i)}\}_{i=1}^T$, learning is accomplished by using mini-batch stochastic gradient descent to minimize the task-dependent loss function $L(\Theta)$ in (2). We adopt a hinge loss for link prediction and mean-squared/absolute error for the edge-weight regression task. For link prediction, we also learn a threshold $t \in \mathbb{R}_+$ to binarize the estimated edge weights and declare presence or absence of edges; see Appendix A.4 for all training-related details including those concerning loss functions.

The iterative refinement principle of optimization algorithms carries over to our GDN model during inference. Indeed, we start with an initial estimate $\mathbf{A}[0] \in \mathcal{A}$ and use a cascade of D linear filters and point-wise non-linearities to refine it to an output $\hat{\mathbf{A}}_L = \Phi(\mathbf{A}_O; \Theta)$; see Fig. 2 for an example drawn from the experiments in Section 5.1. Matrix $\mathbf{A}[0]$ is a hyperparameter we can select to incorporate prior information on the sought latent graph, or it could be learned; see Section 4.3. The input graph \mathbf{A}_O which we aim to deconvolve is directly fed to all layers, defining non-uniform soft thresholds which sparsify the layer’s output. One can also interpret $\alpha\mathbf{A} + \beta(\mathbf{A}_O\mathbf{A} + \mathbf{A}\mathbf{A}_O)$ as a first-order graph filter – here viewed as a signal with N features per node to invoke this GSP insight. In its simplest rendition, the GDN leverages elements of RNNs and graph convolutional networks (GCNs) [45].

4.3 GDN architecture adaptations

Here we outline several customizations and enhancements to the vanilla GDN architecture of the previous section, which we have empirically found to improve graph learning performance.

Incorporating prior information via algorithm initialization. By viewing our method as an iterative refinement of an initial graph $\mathbf{A}[0]$, one can think of $\mathbf{A}[0]$ as a best initial guess, or *prior*, over \mathbf{A}_L . A simple strategy to incorporate prior information about some edge (i, j) , encoded in A_{ij} that we view as a random variable, would be to set $A[0]_{ij} = \mathbb{E}[A_{ij}]$. This technique is adopted when training on the HCP-YA dataset in Section 5, by taking the prior $\mathbf{A}[0]$ to be the sample mean of all latent (i.e., SC) graphs in the training set. This encodes our prior knowledge that there are strong similarities in the structure of the human brain across the population of healthy young adults. When \mathbf{A}_L is expected to be reasonably sparse, we can set $\mathbf{A}[0] = \mathbf{0}$, which is effective as we show in Table 1. Recalling the connections drawn between GDNs and RNNs, then the prior $\mathbf{A}[0]$ plays a similar role to the initial RNN state and thus it could be learned [46]. In any case, the ability to seamlessly incorporate prior information to the model is an attractive feature of GDNs, and differentiates it from other methods trying to solve the network inverse problem.

Multi-Input Multi-Output (MIMO) filters. So far, in each layer we have a single learned filter, which takes an $N \times N$ matrix as input and returns another $N \times N$ matrix at the output. After going through the shifted ReLU nonlinearity, this refined output adjacency matrix is fed as input to the next layer; a process that repeats D times. More generally, we can allow for multiple input channels (i.e., a tensor), as well as multiple channels at the output, by using the familiar convolutional neural network (CNN) methodology. This way, each output channel has its own filter parameters associated with every input channel. The j -th output channel applies its linear filters to all input channels, aggregating the results with a reduction operation (e.g., mean or sum), and applies a point-wise nonlinearity (here a shifted ReLU) to the output. This allows the GDN model to learn many different filters, thus providing richer learned representations and effectively relaxing the simplifying assumption we made regarding a common filter across graph pairs in (1). Full details of MIMO filters are in Appendix A.5.

Decoupling layer parameters. Thus far, we have respected the parameter sharing constraint imposed by the unrolled PG iterations. We now allow each layer to learn a decoupled MIMO filter, with its own set of parameters mapping from C_{in}^k input channels to C_{out}^k output channels. As the notation suggests, C_{in}^k and C_{out}^k need not be equal. By decoupling the layer structure, we allow GDNs to compose different learned filters to create more abstract features (as with CNNs or GCNs). Accordingly, it opens up the architectural design space to broader exploration, e.g., wider layers early and skinnier layers at the end. Exploring this architectural space is beyond the scope of this

paper and is left as future work. In our experiments, we use GDN models for which intermediate layers $k \in \{2, \dots, D - 1\}$ have $C = C_{in}^k = C_{out}^k$, i.e., a flat architecture. We denote models with layer-wise shared parameters and independent parameters as GDN-S and GDN, respectively.

5 Experiments

We present experiments on link prediction and edge-weight regression tasks using synthetic data (Section 5.1), as well as real HCP-YA neuroimaging and social network data (Section 5.2). In the link prediction task, performance is evaluated using error $:= \frac{\text{incorrectly predicted edges}}{\text{total possible edges}}$. For regression, we adopt the mean-squared-error (MSE) or mean-absolute-error (MAE) as figures of merit. In the synthetic data experiments we consider three test cases whereby the latent graphs are respectively drawn from ensembles of Erdős-Rényi (ER), random geometric (RG), and Barabási-Albert (BA) random graph models. We study an additional scenario where we use SCs from HCP-YA (referred to as the ‘pseudo-synthetic’ case because the latent graphs are real structural brain networks). We compare GDNs against several relevant baselines: Network Deconvolution (ND) which uses a spectral approach to directly invert a very specific convolutive mixture [8]; Spectral Templates (SpecTemp) that advocates a convex optimization approach to recover sparse graphs from noisy estimates of A_O ’s eigenvectors [11]; Graphical LASSO (GLASSO), a regularized MLE of the precision matrix for Gaussian graphical model selection [21]; a learned unrolling of AM on the GLASSO objective (GLAD) [32]; least-squares fitting of \mathbf{h} followed by non-convex optimization to solve (3) (LSOpt); and Hard Thresholding (Threshold) to assess how well a simple cutoff rule can perform. The network inverse problem only assumes knowledge of the observed graph A_O for inference - *there is no nodal information available and GDN layers do not operate on node features*. As such, popular GNN based methods used in the link-prediction task [29, 9, 30, 31, 47, 48] cannot be used. Likewise for L2G [33], which advocates a signal smoothness prior. Instead, signals in Section 5.1 are assumed to be graph stationary [12, 11] and filters need not be low-pass. We carefully reviewed the network inference literature and chose the most performant baselines available for this problem setting. Unless otherwise stated, in all the results that follow we use GDN(-S) models with $D = 8$ layers, $C = 8$ channels per layer, take prior $A[0] = \mathbf{0}$ on all domains except the SCs - where we use the sample mean of all SCs in the training set, and train using the Adam optimizer [49] with learning rate of 0.01 and batch size of 200. We use one Nvidia T4 GPU; models take < 15 minutes to train on all datasets.

5.1 Learning graph structure from diffused signals

A set of latent graphs are either sampled from RG, ER, or the BA model, or taken as the SCs from the HCP-YA dataset. In an attempt to make the synthetic latent graphs somewhat comparable to the 68 node SCs, we sample connected $N = 68$ node graphs with edge densities in the range $[0.5, 0.6]$ when feasible – typical values observed in SC graphs. To generate each observation $A_O^{(i)}$, we simulated $P = 50$ standard Normal white signals diffused over $A_L^{(i)}$; from which we form the sample covariance $\hat{\Sigma}_x$ as in Section 3. We let $K = 2$, and sample the filter coefficients $\mathbf{h} \in \mathbb{R}^3$ in $\mathbf{H}(A_L; \mathbf{h})$ uniformly from the unit sphere. To examine robustness to the realizations of \mathbf{h} , we repeat this data generation process three times (resampling the filter coefficients). We thus create three different datasets for each graph domain (12 in total). For the sizes of the training/validation/test splits, the pseudo-synthetic domain uses 913/50/100 and the synthetic domains use 913/500/500.

Table 1 tabulates the results for synthetic and pseudo-synthetic experiments. For graph models that exhibit localized connectivity patterns (RG and SC), GDNs significantly outperform the baselines on both tasks. For the SC test case, GDN (GDN-S) reduces error relative to the mean prior by $27.5 \pm 1.7\%$ ($23.0 \pm 1.7\%$) and MSE by $37.3 \pm 0.8\%$ ($23.2 \pm 0.5\%$). Both GDN architectures show the ability to learn such local patterns, with the extra representational power of GDNs (over GDN-S) providing an additional boost in performance. All models struggle on BA and ER with GDNs showing better performance even for these cases.

Scaling and size generalization: Deploying on larger graphs. GDNs learn the parameters of graph convolutions for the processing of graphs making them inductive: we can deploy the learnt model on larger graph size domains. Such a deployment is feasible on very large graphs due to the $\mathcal{O}(N^2)$ time and memory complexity of GDNs. This stands in contrast to the $\mathcal{O}(N^3)$ time complexity of SpecTemp, GLASSO, ND, and GLAD. SpecTemp and ND perform a full eigendecomposition

Table 1: Mean and standard error of the test performance on both tasks across graph domains. The SC columns are a ‘pseudo-synthetic’ case because the latent graphs are real brain SCs. Left: error (%) on link prediction task. Right: MSE on edge-weight regression task. Bold denotes best performance.

MODELS	RG	ER	BA	SC	RG	ER	BA	SC
GDN	4.6 \pm 4E-1	41.9 \pm 1E-1	27.5 \pm 1E-3	8.9 \pm 2E-2	4.2E-2 \pm 4E-3	2.3E-1 \pm 2E-3	1.8E-1 \pm 2E-3	5.3E-3 \pm 7E-5
GDN-S	5.5 \pm 2E-1	40.8 \pm 1E-2	27.6 \pm 8E-4	9.4 \pm 2E-1	6.0E-2 \pm 2E-1	2.3E-1 \pm 2E-3	2.7E-1 \pm 2E-2	6.5E-3 \pm 4E-5
GLAD	6.3 \pm 2E-1	43.7 \pm 3E-1	35.0 \pm 3E-2	11.8 \pm 2E-3	7.8E-2 \pm 9E-4	2.4E-1 \pm 4E-3	1.9E-1 \pm 4E-3	1.4E-2 \pm 7E-6
GLASSO	8.8 \pm 7E-2	43.2 \pm 1E-2	34.9 \pm 9E-3	20.0 \pm 4E-2	2.0E-1 \pm 3E-3	2.8E-1 \pm 2E-2	2.6E-1 \pm 2E-2	4.4E-2 \pm 3E-5
ND	9.4 \pm 3E-1	43.9 \pm 1E-2	34.1 \pm 8E-3	21.3 \pm 9E-2	1.8E-1 \pm 2E-3	2.4E-1 \pm 5E-4	2.2E-1 \pm 1E-3	5.6E-2 \pm 7E-5
SPECTEMP	11.1 \pm 3E-1	44.4 \pm 7E-2	30.2 \pm 2E-1	30.0 \pm 1E-1	5.1E-2 \pm 3E-5	5.3E-1 \pm 9E-5	3.3E-1 \pm 2E-5	1.5E-1 \pm 4E-3
LSOPT	24.2 \pm 5E-0	42.5 \pm 3E-1	28.0 \pm 2E-1	31.5 \pm 6E-3	9.9E-2 \pm 2E-1	2.5E-1 \pm 2E-3	2.0E-1 \pm 3E-3	6.1E-0 \pm 6E-4
THRESHOLD	12.0 \pm 2E-1	42.9 \pm 8E-1	32.3 \pm 1E-0	21.7 \pm 2E-1				

of \mathbf{A}_O , the iterative algorithms for solving GLASSO incur cubic worst-case complexity [50], and GLAD performs a matrix square root in *each* layer. GLAD also requires deeper unrolled networks, discounted intermediate losses, and multiple embedded MLPs, which have significant practical implications on memory usage; see also Appendix A.8.

To test the extent to which GDNs generalize when N grows, we trained GDN(-S) on RG graphs with size $N = 68$, and tested them on RG graphs of size $N = [68, 75, 100, 200, 500, 1000, 2000]$, with 200 graphs of each size. As graph sizes increase, we require more samples in the estimation of the sample covariance to maintain a constant signal-to-noise ratio. To simplify the experiment and its interpretation, we disregard estimation and directly use the ensemble covariance $\mathbf{A}_O \equiv \Sigma_x$ as observation. As before, we take a training/validation split of 913/500. Figure 3 shows GDNs effectively generalize to graphs orders of magnitude larger than they were trained on, giving up only modest levels of performance as size increases. Note that the best performing baseline in Table 1 - trained *and tested* on the original $N = 68$ domain - is not comparable with GDN-S in terms of performance until GDN-S is tested on graphs almost an order of magnitude larger than those it was trained on. The GDN-S model showed a more graceful performance degradation, suggesting that GDNs without parameter sharing may be using their extra representational power to pick up on finite-size effects, which may disappear as N increases. The shared parameter constraint acts as regularization, we avoid over-fitting on a given size domain to better generalize to larger graphs.

Ablation studies. The choice of prior can influence model performance, as well as reduce training time and the number of parameters needed. When run on stochastic block model (SBM) graphs with $N = 21$ nodes and 3 equally-sized communities (within block connection probability of 0.6, and 0.1 across blocks), for the link prediction task GDNs attain an error of $16.8 \pm 2.7e-2\%$, $16.0 \pm 2.1e-2\%$, $14.5 \pm 1.0e-2\%$, $14.3 \pm 8.8e-2\%$ using a zeros, ones, block diagonal, and learned prior, respectively. The performance improves when GDNs are given an informative prior (here a block diagonal matrix matching the graph communities), with further gains when GDNs are allowed to learn $\mathbf{A}[0]$.

We also study the effect of gradient truncation. To derive GDNs we approximate the gradient $\nabla g(\mathbf{A})$ by dropping all higher-order terms in \mathbf{A} ($K = 1$). The case of $K = 0$ corresponds to further dropping the terms linear in \mathbf{A} , leading to PG iterations $\mathbf{A}[k+1] = \text{ReLU}(\mathbf{A}[k] + \gamma \mathbf{A}_O - \tau \mathbf{1}\mathbf{1}^\top)$ [cf. (6)]. We run this simplified model with $D = 8$ layers and $C = 8$ channels per layer on the same RG graphs in Table 1. Lacking the linear term that facilitates information aggregation in the graph, the model is not expressive enough and yields a higher error (MSE) of $25.7 \pm 1.3e-2\%$ ($1.7e-1 \pm 4.7e-4$) for the link-prediction (edge weight regression) task. Models with $K \geq 2$ result in unstable training, which motivates our choice of $K = 1$ in GDNs.

5.2 Real Data

HCP-YA neuroimaging dataset. HCP represents a unifying paradigm to acquire high quality neuroimaging data across studies that enabled unprecedented quality of macro-scale human brain connectomes for analyses in different domains [51]. We use the dMRI and resting state fMRI data from the HCP-YA dataset [52], consisting of 1200 healthy, young adults (ages: 22-36 years). The SC and FC are projected on a common brain atlas, which is a grouping of cortical structures in the brain to distinct regions. We interpret these regions as nodes in a brain graph. For our experiments, we use the standard Desikan-Killiany atlas [53] with $N = 68$ cortical brain regions. The SC-FC

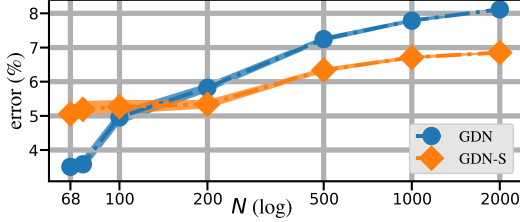


Figure 3: Size Generalization: GDNs maintain performance on RG graphs orders of magnitude larger than the $N = 68$ training set.

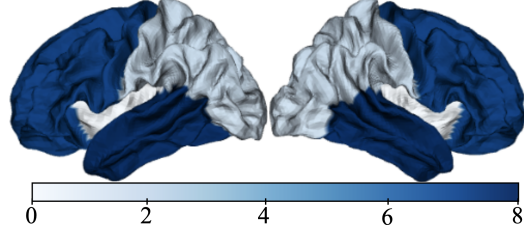


Figure 4: Reduction in MAE (%) for different lobes; largest improvements occur in temporal and frontal lobes.

coupling on this dataset is known to be the strongest in the occipital lobe and vary with age, sex and cognitive health in other subnetworks [39]. Under the consideration of the variability in SC-FC coupling across the brain regions, we further group the cortical regions into 4 neurologically defined ‘lobes’: frontal, parietal, temporal, and occipital (the locations of these lobes in the brain are included in Fig. 6 in Appendix A.7). We aim to predict SC, derived from dMRI, using FC, constructed using BOLD signals acquired with fMRI. In the literature, the forward (SC to FC) problem has been mostly attempted, a non-trivial yet simpler task due to the known reliance of function on structure in many cortical regions. We tackle the markedly harder inverse (deconvolution) problem of recovering SC from FC, which has so far received less attention and can have major impact as described in Section 3.

From this data, we extracted a dataset of 1063 FC-SC pairs, $\mathcal{T} = \{FC^{(i)}, SC^{(i)}\}_{i=1}^{1063}$ and use a training/validation/test split of 913/50/100. Taking the prior $A[0]$ as the edgewise mean over all SCs in the training split \mathcal{T}_{train} : $A[0]_{ij} = \text{mean} \{SC_{i,j}^{(1)}, \dots, SC_{i,j}^{(913)}\}$ and using it directly as a predictor on the test set (tuning a threshold with validation data), we achieve strong performance on link-prediction and edge-weight regression tasks on the whole brain (error = 12.3%, MAE = 0.0615). At the lobe level, the prior achieves relatively higher accuracy in occipital (error = 1.3%, MAE = 0.064) and parietal (error = 6.6%, MAE = 0.07) lobes as compared to temporal (error = 11.0%, MAE = 0.053) and frontal (error = 10.5%, MAE = 0.062) lobes; behavior which is unsurprising as SC in temporal and frontal lobes are affected by ageing and gender related variability in the dataset [54]. GDNs reduced MAE by 7.6%, 7.1%, 1.6%, and 1.3% in the temporal, frontal, parietal, and occipital networks respectively and 8.0% over the entire brain network, all relative to the already strong mean prior. The four lobe reductions are visualized in Figure 4. We observed the most significant gains over temporal and frontal lobes; clearly there was smaller room to improve performance over the occipital and frontal lobes. None of the baseline methods were able to reduce MAE (or error) and hence are not included. The pseudo-synthetic domain can guide interpretation of the relative merits of methods on HCP data, as it is a relaxed version of the same task. Our results justify GDNs as the leading baseline for comparisons in this significant FC to SC task, and we contribute code to facilitate said evaluation. For additional interpretation of HCP-YA results, see Appendix A.7.

Friendship recommendation from physical co-location networks. Here we use GDNs to predict Facebook ties given human co-location data. GDNs are well suited for this deconvolution problem since one can view friendships as direct ties, whereas co-location edges include indirect relationships due to casual encounters in addition to face-to-face contacts with friends. A trained model could then be useful to augment friendship recommendation engines given co-location (behavioral) data; which also poses interesting privacy questions. The Thiers13 dataset [55] monitored high school students, recording (i) physical co-location interactions with wearable sensors over 5 days; and (ii) social network information via survey. From this we construct a dataset \mathcal{T} of graph pairs, each with $N = 120$ nodes, where A_O are co-location networks, i.e., weighted graphs where the weight of edge (i, j) represents the number of times student i and j came into physical proximity, and A_L is the Facebook subgraph between the same students; further details are in Appendix A.7. We trained a GDN of depth $D = 11$ without MIMO filters ($C = 1$), with learned $A[0]$ using a training/validation/test split of 5000/1000/1000. We achieved a test error of $8.9 \pm 1.5e-2\%$, a 13.0% reduction over next best performing baseline (see Appendix A.7), suggesting we learn a latent mechanism that the baselines (even GLAD, a supervised graph learning method) cannot.

6 Conclusions

In this work we proposed the GDN, an inductive model capable of recovering latent graph structure from observations of its convolutional mixtures. By minimizing a task-dependent loss function, GDNs learn filters to refine initial estimates of the sought latent graphs layer by layer. The unrolled architecture can seamlessly integrate domain-specific prior information about the unknown graph distribution. Moreover, because GDNs: (i) are differentiable functions with respect to their parameters as well as their graph input; and (ii) offer explicit control on complexity (leading to fast inference times); one can envision GDNs as valuable components in larger (even online) end-to-end graph representation learning systems. This way, while our focus here has been exclusively on network topology identification, the impact of GDNs can permeate to broader graph inference tasks.

References

- [1] Michael M Bronstein, Joan Bruna, Yann LeCun, Arthur Szlam, and Pierre Vandergheynst. Geometric deep learning: going beyond Euclidean data. *IEEE Signal Process. Mag.*, 34(4): 18–42, 2017.
- [2] Antonio Ortega, Pascal Frossard, Jelena Kovačević, José M. F. Moura, and Pierre Vandergheynst. Graph signal processing: Overview, challenges, and applications. *Proc. IEEE*, 106(5):808–828, 2018.
- [3] Xiaowen Dong, Dorina Thanou, Michael Rabbat, and Pascal Frossard. Learning graphs from data: A signal representation perspective. *IEEE Signal Process. Mag.*, 36(3):44–63, 2019.
- [4] Gonzalo Mateos, Santiago Segarra, Antonio G. Marques, and Alejandro Ribeiro. Connecting the dots: Identifying network structure via graph signal processing. *IEEE Signal Process. Mag.*, 36(3):16–43, May 2019.
- [5] Georgios B. Giannakis, Yanning Shen, and Georgios Vasileios Karanikolas. Topology identification and learning over graphs: Accounting for nonlinearities and dynamics. *Proceedings of the IEEE*, 106(5):787–807, 2018.
- [6] William L. Hamilton. Graph representation learning. *Synthesis Lectures on Artificial Intelligence and Machine Learning*, 14(3):1–159, 2020.
- [7] Fernando Gama, Joan Bruna, and Alejandro Ribeiro. Stability properties of graph neural networks. *IEEE Trans. Signal Process.*, 68:5680–5695, 2020.
- [8] Soheil Feizi, Daniel Marbach, Muriel Medard, and Manolis Kellis. Network deconvolution as a general method to distinguish direct dependencies in networks. *Nat. Biotechnol.*, 31(8):726–733, 2013.
- [9] Anees Kazi, Luca Cosmo, Nassir Navab, and Michael M. Bronstein. Differentiable graph module (DGM) for graph convolutional networks. *CoRR*, abs/2002.04999, 2020. URL <https://arxiv.org/abs/2002.04999>.
- [10] Daniel A. Spielman and Nikhil Srivastava. Graph sparsification by effective resistances. *SIAM J. Comput.*, 40(6):1913–1926, December 2011.
- [11] Santiago Segarra, Antonio G. Marques, Gonzalo Mateos, and Alejandro Ribeiro. Network topology inference from spectral templates. *IEEE Trans. Signal Inf. Process. Netw.*, 3(3): 467–483, August 2017.
- [12] Bastien Paudeloup, Vincent Gripon, Grégoire Mercier, Dominique Pastor, and Michael G. Rabbat. Characterization and inference of graph diffusion processes from observations of stationary signals. *IEEE Trans. Signal Inf. Process. Netw.*, 4(3):481–496, 2018.
- [13] Karol Gregor and Yann LeCun. Learning fast approximations of sparse coding. In *International Conference on Machine Learning*, page 399–406, 2010.
- [14] P. Sprechmann, A. M. Bronstein, and G. Sapiro. Learning efficient sparse and low rank models. *IEEE Trans. Pattern Anal. Mach. Intell.*, 37(9):1821–1833, 2015.
- [15] Vishal Monga, Yuelong Li, and Yonina C. Eldar. Algorithm unrolling: Interpretable, efficient deep learning for signal and image processing. *IEEE Signal Process. Mag.*, 38(2):18–44, 2021.

- [16] Gilad Yehudai, Ethan Fetaya, Eli Meir, Gal Chechik, and Haggai Maron. From local structures to size generalization in graph neural networks. In *International Conference on Machine Learning*, pages 11975–11986. PMLR, 2021.
- [17] F. Abdelnour, H. U. Voss, and A. Raj. Network diffusion accurately models the relationship between structural and functional brain connectivity networks. *Neuroimage*, 90:335–347, Apr. 2014.
- [18] Hualou Liang and Hongbin Wang. Structure-function network mapping and its assessment via persistent homology. *PLOS Comput. Biol.*, 13(e1005325):1–19, Jan. 2017.
- [19] Arthur P Dempster. Covariance selection. *Biometrics*, pages 157–175, 1972.
- [20] E. D. Kolaczyk. *Statistical Analysis of Network Data: Methods and Models*. Springer, New York, NY, 2009.
- [21] J. Friedman, T. Hastie, and R. Tibshirani. Sparse inverse covariance estimation with the graphical lasso. *Biostatistics*, 9(3):432–441, 2008.
- [22] Mathias Drton and Marloes H Maathuis. Structure learning in graphical modeling. *Annu. Rev. Stat. Appl.*, 4:365–393, 2017.
- [23] Hadi Daneshmand, Manuel Gomez-Rodriguez, Le Song, and Bernhard Schoelkopf. Estimating diffusion network structures: Recovery conditions, sample complexity & soft-thresholding algorithm. In *International Conference on Machine Learning*, pages 793–801. PMLR, 2014.
- [24] Xiaowen Dong, Dorina Thanou, Pascal Frossard, and Pierre Vandergheynst. Learning laplacian matrix in smooth graph signal representations. *IEEE Trans. Signal Process.*, 64(23):6160–6173, 2016.
- [25] Vassilis Kalofolias. How to learn a graph from smooth signals. In *Artificial Intelligence and Statistics*, pages 920–929, 2016.
- [26] Renjie Liao, Yujia Li, Yang Song, Shenlong Wang, Charlie Nash, William L. Hamilton, David Duvenaud, Raquel Urtasun, and Richard Zemel. Efficient graph generation with graph recurrent attention networks. In *Advances in Neural Information Processing Systems*, 2019.
- [27] Hongwei Wang, Jia Wang, Jialin Wang, Miao Zhao, Weinan Zhang, Fuzheng Zhang, Xing Xie, and Minyi Guo. GraphGAN: Graph representation learning with generative adversarial nets. In *AAAI Conference on Artificial Intelligence*, pages 2508–2515, 2018.
- [28] Yujia Li, Oriol Vinyals, Chris Dyer, Razvan Pascanu, and Peter Battaglia. Learning deep generative models of graphs. *CoRR*, abs/1803.03324, 2018. URL <https://arxiv.org/abs/1803.03324>.
- [29] Yue Wang, Yongbin Sun, Ziwei Liu, Sanjay E. Sarma, Michael M. Bronstein, and Justin M. Solomon. Dynamic graph CNN for learning on point clouds. *ACM Trans. Graph.*, 38(5), October 2019.
- [30] Petar Veličković, Lars Buesing, Matthew C. Overlan, Razvan Pascanu, Oriol Vinyals, and Charles Blundell. Pointer graph networks. In *Advances in Neural Information Processing Systems*, 2020.
- [31] Thomas Kipf, Ethan Fetaya, Kuan-Chieh Wang, Max Welling, and Richard Zemel. Neural relational inference for interacting systems. In *International Conference on Machine Learning*, volume 80, pages 2688–2697, 10–15 Jul 2018.
- [32] Harsh Shrivastava, Xinshi Chen, Binghong Chen, Guanghui Lan, Srinvas Aluru, Han Liu, and Le Song. Glad: Learning sparse graph recovery, 2019.
- [33] Xingyue Pu, Tianyue Cao, Xiaoyun Zhang, Xiaowen Dong, and Siheng Chen. Learning to learn graph topologies, 2021.
- [34] Fernando Gama, Elvin Isufi, Geert Leus, and Alejandro Ribeiro. Graphs, convolutions, and neural networks: From graph filters to graph neural networks. *IEEE Signal Process. Mag.*, 37(6):128–138, 2020.
- [35] Alain Barrat, Marc Barthelemy, and Alessandr Vespignani. *Dynamical Processes on Complex Networks*. Cambridge University Press, New York, NY, 2008.
- [36] Morris H. DeGroot. Reaching a consensus. *J Am Stat Assoc.*, 69:118–121, 1974.

- [37] C. H. Yeh, D. K. Jones, X. Liang, M. Descoteaux, and A. Connelly. Mapping structural connectivity using diffusion mri: Challenges and opportunities. *J. Magn. Reson.*, 53(6):1666–1682, 2021.
- [38] C. Honey, O. Sporns, L. Cammoun, X. Gigandet, J. Thiran, R. Meuli, and P. Hagmann. Predicting human resting-state functional connectivity from structural connectivity. *Proc. Natl. Acad. Sci. U.S.A.*, 106:2035–2040, 2009.
- [39] Zijin Gu, Keith Wakefield Jamison, Mert Rory Sabuncu, and Amy Kuceyeski. Heritability and interindividual variability of regional structure-function coupling. *Nat. Commun.*, 12(1):1–12, 2021.
- [40] Michael Greicius, Kaustubh Supekar, Vinod Menon, and Robert Dougherty. Resting-state functional connectivity reflects structural connectivity in the default mode network. *Cereb Cortex*, 19:72–8, 12 2008.
- [41] Jessica S Damoiseaux and Michael D Greicius. Greater than the sum of its parts: A review of studies combining structural connectivity and resting-state functional connectivity. *Brain Struct. Func.*, 213(6):525–533, 2009.
- [42] Jérôme Bolte, Shoham Sabach, Marc Teboulle, and Yakov Vaisbourd. First order methods beyond convexity and Lipschitz gradient continuity with applications to quadratic inverse problems. *SIAM J. Optim.*, 28(3):2131–2151, 2018.
- [43] Junyu Zhang and Mingyi Hong. First-order algorithms without Lipschitz gradient: A sequential local optimization approach. *CoRR*, abs/2010.03194, 2020. URL <https://arxiv.org/abs/2010.03194>.
- [44] Neal Parikh and Stephen Boyd. Proximal algorithms. *Foundations and Trends in Optimization*, 1(3):127–239, 2014.
- [45] Thomas N. Kipf and Max Welling. Semi-supervised classification with graph convolutional networks. In *International Conference on Learning Representations*, 2017.
- [46] Geoffrey E. Hinton. Advanced machine learning: Recurrent neural networks, 2013. URL <https://www.cs.toronto.edu/~hinton/csc2535/notes/lec10new.pdf>.
- [47] Thomas N. Kipf and Max Welling. Variational graph auto-encoders, 2016. URL <https://arxiv.org/abs/1611.07308>.
- [48] Muhan Zhang and Yixin Chen. Link prediction based on graph neural networks, 2018. URL <https://arxiv.org/abs/1802.09691>.
- [49] Diederik P Kingma and Jimmy Ba. Adam: A method for stochastic optimization. In *ICLR (Poster)*, 2015.
- [50] Richard Zhang, Salar Fattahi, and Somayeh Sojoudi. Large-scale sparse inverse covariance estimation via thresholding and max-det matrix completion. In *International Conference on Machine Learning*, pages 5766–5775. PMLR, 2018.
- [51] Matthew F Glasser, Stephen M Smith, Daniel S Marcus, Jesper LR Andersson, Edward J Auerbach, Timothy EJ Behrens, Timothy S Coalson, Michael P Harms, Mark Jenkinson, Steen Moeller, et al. The human connectome project’s neuroimaging approach. *Nature neuroscience*, 19(9):1175–1187, 2016.
- [52] David C Van Essen, Stephen M Smith, Deanna M Barch, Timothy EJ Behrens, Essa Yacoub, Kamil Ugurbil, Wu-Minn HCP Consortium, et al. The WU-Minn Human Connectome Project: An overview. *Neuroimage*, 80:62–79, 2013.
- [53] Rahul S Desikan, Florent Ségonne, Bruce Fischl, Brian T Quinn, Bradford C Dickerson, Deborah Blacker, Randy L Buckner, Anders M Dale, R Paul Maguire, Bradley T Hyman, et al. An automated labeling system for subdividing the human cerebral cortex on mri scans into gyral based regions of interest. *Neuroimage*, 31(3):968–980, 2006.
- [54] Joelle Zimmermann, Petra Ritter, Kelly Shen, Simon Rothmeier, Michael Schirner, and Anthony R McIntosh. Structural architecture supports functional organization in the human aging brain at a regionwise and network level. *Hum. Brain Mapp*, 37(7):2645–2661, 2016.
- [55] Mathieu Génois and Alain Barrat. Can co-location be used as a proxy for face-to-face contacts? *EPJ Data Science*, 7(1):11, May 2018.

- [56] Ming Yuan and Yi Lin. Model selection and estimation in the Gaussian graphical model. *Biometrika*, 94(1):19–35, 2007.
- [57] Adam Paszke, Sam Gross, Francisco Massa, Adam Lerer, James Bradbury, Gregory Chanan, Trevor Killeen, Zeming Lin, Natalia Gimelshein, Luca Antiga, Alban Desmaison, Andreas Kopf, Edward Yang, Zachary DeVito, Martin Raison, Alykhan Tejani, Sasank Chilamkurthy, Benoit Steiner, Lu Fang, Junjie Bai, and Soumith Chintala. Pytorch: An imperative style, high-performance deep learning library. In H. Wallach, H. Larochelle, A. Beygelzimer, F. d’Alché-Buc, E. Fox, and R. Garnett, editors, *Advances in Neural Information Processing Systems 32*, pages 8024–8035. Curran Associates, Inc., 2019. URL <http://papers.neurips.cc/paper/9015-pytorch-an-imperative-style-high-performance-deep-learning-library.pdf>.
- [58] Anaconda software distribution, 2020. URL <https://docs.anaconda.com/>.

A Appendix

A.1 Model Identifiability

Without any constraints on \mathbf{h} and \mathbf{A}_L , the problem of recovering \mathbf{A}_L from $\mathbf{A}_O = \mathbf{H}(\mathbf{A}_L; \mathbf{h})$ as in (1) is clearly non-identifiable. Indeed, if the desired solution is \mathbf{A}_L (with associated polynomial coefficients \mathbf{h}), there is always at least another solution \mathbf{A}_O corresponding to the identity polynomial mapping. This is why adding structural constraints like sparsity on \mathbf{A}_L will aid model identifiability, especially when devoid of training examples.

It is worth mentioning that (1) implies the eigenvectors of \mathbf{A}_L and \mathbf{A}_O coincide. So the eigenvectors of the sought latent graph are given once we observe \mathbf{A}_O , what is left to determine are the eigenvalues. We have in practice observed that for several families of sparse, weighted graphs, the eigenvector information along with the constraint $\mathbf{A}_L \in \mathcal{A}$ are sufficient to uniquely specify the graph. Interestingly, this implies that many random weighted graphs can be uniquely determined from their eigenvectors. This strong uniqueness result does not render our problem vacuous, since seldomly in practice one gets to observe \mathbf{A}_O (and hence its eigenvectors) error free.

If one were to formally study identifiability of (1) (say under some structural assumptions on \mathbf{A}_L and/or the polynomial mapping), then one has to recognize the problem suffers from an inherent scaling ambiguity. Indeed, if given $\mathbf{A}_O = \mathbf{H}(\mathbf{A}_L; \mathbf{h})$ which means the pair \mathbf{A}_L and $\mathbf{h} = [h_0, h_1, \dots, h_K]^\top$ is a solution, then for any positive scalar α one has that $\alpha\mathbf{A}_L$ and $[h_0, h_1/\alpha, \dots, h_K/(\alpha^K)]^\top$ is another solution. Accordingly, uniqueness claims can only be meaningful modulo this unavoidable scaling ambiguity. But this ambiguity is lifted once we tackle the problem in a supervised learning fashion – our approach in this paper. The training samples in $\mathcal{T} := \{\mathbf{A}_O^{(i)}, \mathbf{A}_L^{(i)}\}_{i=1}^T$ fix the scaling, and accordingly the GDN can learn the mechanism or mapping of interest $\mathbf{A}_O \mapsto \mathbf{A}_L$. Hence, an attractive feature of the GDN approach is that by using data, some of the inherent ambiguities in (1) are naturally overcome. In particular, the SpecTemp approach in [11] relies on convex optimization and suffers from this scaling ambiguity, so it requires an extra (rather arbitrary) constraint to fix the scale. The network deconvolution approach in [8] relies on a fixed, known polynomial mapping, and while it does not suffer from these ambiguities it is limited in the graph convolutions it can model.

All in all, the inverse problem associated to (1) is just our starting point to motivate a trainable parametrized architecture $\hat{\mathbf{A}}_L = \Phi(\mathbf{A}_O; \Theta)$, that introduces valuable inductive biases to generate graph predictions. The problem we end up solving is different (recall the formal statement in Section 2) because we rely on supervision using graph examples, thus rendering many of these challenging uniqueness questions less relevant.

A.2 Graph Convolutional Model in Context

To further elaborate on the relevance and breadth of applicability of the graph convolutional (or network diffusion) signal model $\mathbf{x} = \mathbf{H}(\mathbf{A}_L; \mathbf{h})\mathbf{w}$, we would like to elucidate connections with related work for graph structure identification. Note that while we used the diffusion-based generative model for our derivations in Section 3, we do not need it as an actual mechanistic process. Indeed,

like in (1) the only thing we ask is for the data covariance $\mathbf{A}_O = \Sigma_x$ to be some analytic function of the latent graph \mathbf{A}_L . This is not extraneous to workhorse statistical methods for topology inference, which (implicitly) make specific choices for these mappings, e.g. (i) correlation networks [20, Ch. 7] rely on the identity mapping $\Sigma_x = \mathbf{A}_L$; (ii) Gaussian graphical model selection methods, such as graphical lasso in [56, 21], adopt $\Sigma_x = \mathbf{A}_L^{-1}$; and (iii) undirected structural equation models $\mathbf{x} = \mathbf{A}_L \mathbf{x} + \mathbf{w}$ which implies $\Sigma_x = (\mathbf{I} - \mathbf{A}_L)^{-2}$ [4]. Accordingly, these models are subsumed by the general framework we put forth here.

A.3 Incorporating Prior Information

In Section 4.3 we introduce the concept of using prior information in the training of GDNs. We do so by encoding information we may have about the unknown latent graph \mathbf{A}_L into $\mathbf{A}[O]$, the starting matrix which GDNs iteratively refine. If the \mathbf{A}_L 's are repeated instances of a graph with fixed nodes, as is the case with the SCs with respect to the 68 fixed brain regions, a simple strategy to incorporate prior information about some edge $\mathbf{A}_{L_{i,j}}$, now viewed as a random variable, would be $\mathbf{A}_{0_{i,j}} \leftarrow \mathbb{E}[\mathbf{A}_{L_{i,j}}]$. But there is more that can be done. We also can estimate the variance $\text{Var}(\mathbf{A}_{L_{i,j}})$, and use it during the training of a GDN, for example taking $\mathbf{A}_{0_{i,j}} \leftarrow \mathcal{N}(\mathbb{E}[\mathbf{A}_{L_{i,j}}], \text{Var}(\mathbf{A}_{L_{i,j}}))$, or even simpler, using a resampling technique and taking $\mathbf{A}_{0_{i,j}}$ to be a random sample in the training set. By doing so, we force the GDN to take into account the distribution and uncertainty in the data, possibly leading to richer learned representations and better performance. It also would act as a form of regularization, not allowing the model to converge on the naive solution of outputting the simple expectation prior, a likely local minimum in training space.

A.4 Training

Training of the GDN model will be performed using stochastic (mini-batch) gradient descent to minimize a task-dependent loss function $L(\Theta)$ as in (2). The loss is defined either as (i) the edgewise squared/absolute error between the predicted graph and the true graph for regression tasks, or (ii) a hinge loss with parameter $\gamma \geq 0$, both averaged over a training set $\mathcal{T} := \{\mathbf{A}_O^{(i)}, \mathbf{A}_L^{(i)}\}_{i=1}^T$, namely

$$\begin{aligned} \ell_{\text{hinge}}(\mathbf{A}_L^{(i)}, \Phi(\mathbf{A}_O^{(i)}; \Theta)) &:= \sum_{i,j} \begin{cases} (\Phi(\mathbf{A}_O^{(i)}; \Theta)_{i,j} - \gamma)^+ & \mathbf{A}_{L_{i,j}} = 0 \\ (-\Phi(\mathbf{A}_O^{(i)}; \Theta)_{i,j} + 1 - \gamma)^+ & \mathbf{A}_{L_{i,j}} > 0 \end{cases}, \\ \ell_{\text{mse}}(\mathbf{A}_L^{(i)}, \Phi(\mathbf{A}_O^{(i)}; \Theta)) &:= \frac{1}{2} \left\| \mathbf{A}_L^{(i)} - \Phi(\mathbf{A}_O^{(i)}; \Theta) \right\|_2^2, \\ \ell_{\text{mae}}(\mathbf{A}_L^{(i)}, \Phi(\mathbf{A}_O^{(i)}; \Theta)) &:= \left\| \mathbf{A}_L^{(i)} - \Phi(\mathbf{A}_O^{(i)}; \Theta) \right\|_1, \\ L(\Theta) &:= \frac{1}{T} \sum_{i \in \mathcal{T}} \ell_u(\mathbf{A}_L^{(i)}, \Phi(\mathbf{A}_O^{(i)}; \Theta)), \quad u \in \{\text{hinge}, \text{mse}, \text{mae}\}. \end{aligned}$$

The loss is optimized with adam using a learning rate of 0.01, $\beta_1 = 0.85$, and $\beta_2 = 0.99$.

Link prediction with GDNs and unbiased estimates of generalization. In the edge-weight regression task, GDNs only use their validation data to determine when training has converged. When performing link-prediction, GDNs have an additional use for this data: to choose the cutoff threshold $t \in \mathbb{R}_+$, determining which raw outputs (which are continuous) should be considered positive edge predictions, *at the end of training*.

We use the training set to learn the parameters (via gradient descent) *and* to tune t . During the validation step, when then use this train-set-tuned- t on the validation data, giving an estimate of generalization error. This is then used for early-stopping, determining the best model learned after training, etc. We do not use the validation data to tune t during training. Only after training has completed, do we tune t with validation data. We train a handful of models this way, and the model which produces the best validation score (in this case lowest error) is the tested with the validation-tuned- t , thus providing an unbiased estimate of generalization.

A.5 MIMO Model Architecture

MIMO filters. Formally, the more expressive GDN architecture with MIMO (Multi-Input Multi-Output) filters is constructed as follows. At layer k of the NN, we take a three-way tensor $\mathbf{A}_k \in \mathbb{R}_+^{C \times N \times N}$ and produce $\mathbf{A}_{k+1} \in \mathbb{R}_+^{C \times N \times N}$, where C is the common number of input and output channels. The assumption of having a common number of input and output channels can be relaxed, as we argue below. By defining multiplication between tensors $\mathbf{T}, \mathbf{B} \in \mathbb{R}^{C \times N \times N}$ as batched matrix multiplication: $[\mathbf{TB}]_{j,:,:} := \mathbf{T}_{j,:,:} \mathbf{B}_{j,:,:}$, and tensor-vector addition and multiplication as $\mathbf{T} + \mathbf{v} := \mathbf{T} + [v_1 \mathbf{1} \mathbf{1}^\top; \dots; v_C \mathbf{1} \mathbf{1}^\top]$ and $[v \mathbf{T}]_{j,:,:} := v_j \mathbf{T}_{j,:,:}$ respectively for $v \in \mathbb{R}^C$, all operations extend naturally.

Using these definitions, the j -th output slice of layer k is

$$[\mathbf{A}_{k+1}]_{j,:,:} = \text{ReLU}[\overline{\alpha_{:,j} \mathbf{A}_k + \beta_{:,j} (\mathbf{A}_O \mathbf{A}_k + \mathbf{A}_k \mathbf{A}_O) + \gamma_{:,j} \mathbf{A}_O} - \tau_j \mathbf{1} \mathbf{1}^\top], \quad (7)$$

where $\overline{\cdot}$ represents the mean reduction over the filtered input channels and the parameters are $\alpha, \beta, \gamma \in \mathbb{R}^{C \times C}$, $\tau \in \mathbb{R}_+^C$. We now take $\Theta := \{\alpha, \beta, \gamma, \tau\}$ for a total of $C \times (3C + 1)$ trainable parameters.

We typically have a single prior matrix $\mathbf{A}[0]$ and are interested in predicting a single adjacency matrix $\hat{\mathbf{A}}_L$. Accordingly, we construct a new tensor prior $\mathbf{A}[0] := [\mathbf{A}[0], \dots, \mathbf{A}[0]] \in \mathbb{R}^{C \times N \times N}$ and (arbitrarily) designate the first output channel as our prediction $\hat{\mathbf{A}}_L = \Phi(\mathbf{A}_O; \Theta) = [\mathbf{A}_{k+1}]_{1,:,:}$.

We can also allow each layer to learn a decoupled MIMO filter, with its own set of parameters mapping from C_{in}^k input channels to C_{out}^k output channels. As the notation suggests, C_{in}^k and C_{out}^k need not be equal. Layer k now has its own set of parameters $\Theta^k = (\alpha^k, \beta^k, \gamma^k, \tau^k)$, where $\alpha^k, \beta^k, \gamma^k \in \mathbb{R}^{C_{out}^k \times C_{in}^k}$ and $\tau^k \in \mathbb{R}_+^{C_{out}^k}$, for a total of $C_{out}^k \times (3C_{in}^k + 1)$ trainable parameters. The tensor operations mapping inputs to outputs remains basically unchanged with respect to (7), except that the filter coefficients will depend on k .

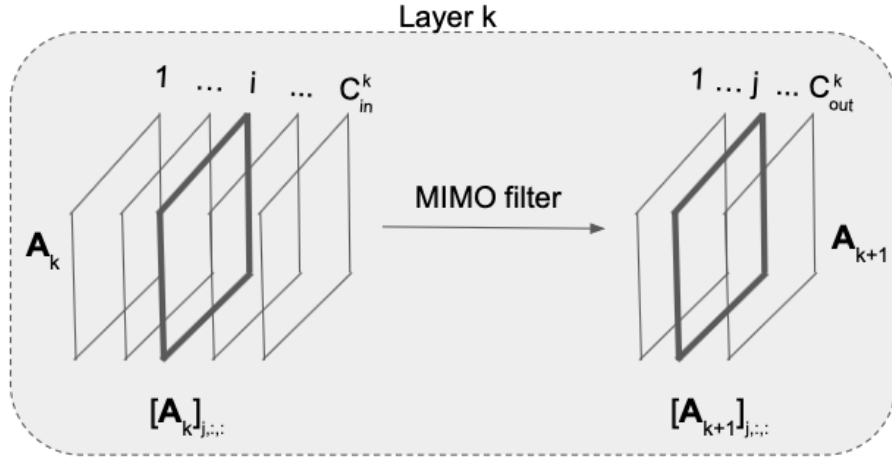


Figure 5: MIMO Filter: Layer k takes a tensor $\mathbf{A}_k \in \mathbb{R}^{C_{in}^k \times N \times N}$ and outputs a tensor $\mathbf{A}_{k+1} \in \mathbb{R}^{C_{out}^k \times N \times N}$. The i -th slice $[\mathbf{A}_k]_{i,:,:}$ is called the i -th input channel and $[\mathbf{A}_{k+1}]_{j,:,:}$ is called the j -th output channel.

Processing at a generic layer k is depicted in Figure 5. Output channel j will use $\alpha_{:,j}^k, \beta_{:,j}^k, \gamma_{:,j}^k \in \mathbb{R}^{C_{in}^k}$ and $\tau_j^k \in \mathbb{R}_+$ to filter all input channels $i \in \{1, \dots, C_{in}^k\}$, which are collected in the input tensor $\mathbf{A}_k \in \mathbb{R}^{C_{in}^k \times N \times N}$. This produces a tensor of stacked filtered input channels $\in \mathbb{R}^{C_{in}^k \times N \times N}$. After setting the diagonal elements of all matrix slices in this tensor to 0, then perform a mean reduction edgewise (over the first mode/dimension) of this tensor, producing a single $N \times N$ matrix. We then apply two pointwise/elementwise operations on this matrix: (i) subtract τ_j^k (this would be the ‘bias’ term in CNNs); and (ii) apply a point-wise nonlinearity (ReLU). This produces an $N \times N$ activation stored in the j -th output channel. Doing so for all output channels $j \in \{1, \dots, C_{out}^k\}$, produces a tensor $\mathbf{A}_{k+1} \in \mathbb{R}^{C_{out}^k \times N \times N}$.

Layer output normalization and zeroing diagonal. The steps not shown in the main text are the normalization steps, a practical issue, and the setting of the diagonal elements to be 0, a projection onto the set \mathcal{A} of allowable adjacency matrices. Define $\bar{\mathbf{U}}_{j,:} = \alpha_{:,j}^k \mathbf{A}_k + \beta_{:,j}^k (\mathbf{A}_O \mathbf{A}_k + \mathbf{A}_k \mathbf{A}_O) + \gamma_{:,j}^k \mathbf{A}_O \in \mathbb{R}^{N \times N}$ as the j -th slice in the intermediate tensor $\bar{\mathbf{U}} \in \mathbb{R}^{C_{out} \times N \times N}$ used in the filtering of \mathbf{A}_k . Normalization is performed by dividing each matrix slice of $\bar{\mathbf{U}}$ by the maximum magnitude element in that respective slice: $\bar{\mathbf{U}}_{:,j} / \max |\bar{\mathbf{U}}_{:,j}|$.

Multiple normalization metrics were tried on the denominator, including the 99th percentile of all values in $\bar{\mathbf{U}}_{:,j}$, the Frobenius norm $\|\bar{\mathbf{U}}_{:,j}\|_F$, among others. None seemed to work as well as the maximum magnitude element, which has the additional advantage of guaranteeing entries to be in $[0, 1]$ (after ReLU), which matches nicely with: (i) adjacency matrices of unweighted graphs; and (ii) makes it easy to normalize edge weights of a dataset of adjacencies: simply scale them to $[0, 1]$. In summary, the full procedure to produce $[\mathbf{A}_{k+1}]_{j,:}$ is as follows:

$$\begin{aligned} \bar{\mathbf{U}}_{j,:} &= \alpha_{:,j}^k \mathbf{A}_k + \beta_{:,j}^k (\mathbf{A}_O \mathbf{A}_k + \mathbf{A}_k \mathbf{A}_O) + \gamma_{:,j}^k \mathbf{A}_O \\ \bar{\mathbf{U}}_{j,:} &= \bar{\mathbf{U}}_{j,:} \odot (\mathbf{1}\mathbf{1}^\top - \mathbf{I}) && \text{force diagonal elements to 0} \\ \bar{\mathbf{U}}_{j,:} &= \bar{\mathbf{U}}_{j,:} / \max(|\bar{\mathbf{U}}_{j,:}|) && \text{normalize entries per slice to be in } [-1, 1] \\ [\mathbf{A}_{k+1}]_{j,:} &= \text{ReLU}(\bar{\mathbf{U}}_{j,:} - \tau_l^j) \end{aligned}$$

By normalizing in this way, we guarantee the intermediate matrix $\bar{\mathbf{U}}_{j,:}$ has entries in $[-1, 1]$ (before the ReLU). This plays two important roles. The first one has to do with training stability and to appreciate this point consider what could happen if no normalization is used. Suppose the entries of $\bar{\mathbf{U}}_{j,:}$ are orders of magnitude larger than entries of $\bar{\mathbf{U}}_{l,:}$. This can cause the model to push $\tau_j^k \gg \tau_l^k$, leading to training instabilities and/or lack of convergence. The second point relates to interpretability of τ . Indeed, the proposed normalization allows us to interpret the learned values $\tau^k \in \mathbb{R}_{out,+}^k$ on a similar scale. All the thresholds must be in $[0, 1]$ because: (i) anything above 1 will make the output all 0; and (ii) we constrain it to be non-negative. In fact we can now plot all τ values (from all layers) against one another, and using the same scale ($[0, 1]$) interpret if a particular τ is promoting a lot of sparsity in the output (τ close to 1) or not (τ close to 0), by examining its magnitude.

A.6 Gradient used in Proximal Gradient Iterations

Here we give mathematical details in the calculation of the gradient $\nabla g(\mathbf{A})$ of the component function $g(\mathbf{A}) := \frac{1}{2} \|\mathbf{A}_O - \mathbf{H}(\mathbf{A}; \mathbf{h})\|_F^2$. Let \mathbf{A}, \mathbf{A}_O be symmetric $N \times N$ matrices and recall the graph filter $\mathbf{H}(\mathbf{A}) := \sum_{k=0}^K h_k \mathbf{A}^k$ (we drop the dependency in \mathbf{h} to simply the notation). Then

$$\begin{aligned} \nabla_{\mathbf{A}} \frac{1}{2} \|\mathbf{A}_O - \mathbf{H}(\mathbf{A})\|_F^2 &= \frac{1}{2} \nabla_{\mathbf{A}} \text{Tr}(\mathbf{A}_O^2 - \mathbf{A}_O \mathbf{H}(\mathbf{A}) - \mathbf{H}(\mathbf{A}) \mathbf{A}_O + \mathbf{H}^2(\mathbf{A})) \\ &= -\nabla_{\mathbf{A}} \text{Tr}(\mathbf{A}_O \mathbf{H}(\mathbf{A})) + \frac{1}{2} \nabla_{\mathbf{A}} \text{Tr} \mathbf{H}^2(\mathbf{A}) \\ &= -\sum_{k=1}^K h_k \sum_{r=0}^{k-1} \mathbf{A}^{k-r-1} \mathbf{A}_O \mathbf{A}^r + \frac{1}{2} \nabla_{\mathbf{A}} \text{Tr} \mathbf{H}^2(\mathbf{A}) \\ &= -\sum_{k=1}^K h_k \sum_{r=0}^{k-1} \mathbf{A}^{k-r-1} \mathbf{A}_O \mathbf{A}^r + \frac{1}{2} \mathbf{H}_1(\mathbf{A}) \\ &= -[h_1 \mathbf{A}_O + h_2 (\mathbf{A} \mathbf{A}_O + \mathbf{A}_O \mathbf{A}) + h_3 (\mathbf{A}^2 \mathbf{A}_O + \mathbf{A} \mathbf{A}_O \mathbf{A} + \mathbf{A}_O \mathbf{A}^2) + \dots] \\ &\quad + \frac{1}{2} \mathbf{H}_1(\mathbf{A}), \end{aligned}$$

where in arriving at the second equality we relied on the cyclic property of the trace, and $\mathbf{H}_1(\mathbf{A})$ is a matrix polynomial of order $2K - 1$.

Note that in the context of the GDN model, powers of \mathbf{A} will lead to complex optimization landscapes, and thus unstable training. We thus opt to drop the higher-order terms and work with a first-order approximation of ∇g , namely

$$\nabla g(\mathbf{A}) \approx -h_1 \mathbf{A}_O - h_2 (\mathbf{A}_O \mathbf{A} + \mathbf{A} \mathbf{A}_O) + (2h_0 h_2 + h_1^2) \mathbf{A}.$$

A.7 Notes on the Experimental Setup

Synthetic graphs. For the experiments presented in Table 1, the synthetic graphs of size $N = 68$ are drawn from random graph models with the following parameters

- Random geometric graphs (RG): $d = 2, r = 0.56$.
- Erdős-Rényi (ER): $p = .56$.
- Barabási-Albert (BA): $m = 15$

When sampling graphs to construct the datasets, we reject any samples which are not connected or have edge density outside of a given range. For RG and ER, that range is $[0.5, 0.6]$, while in BA the range is $[0.3, 0.4]$. This is an attempt to make the RG and ER graphs similar to the brain SC graphs, which have an average edge density of 0.56, and all SCs are in edge density range $[0.5, 0.6]$. Due to the sampling procedure of BA, it is not possible to produce graph in this sparsity range, so we lowered the range slightly. We thus take SCs to be an SBM-like ensemble and avoid a repetitive experiment with randomly drawn SBM graphs.

Note that the edge density ranges define the performance of the most naive of predictors: all ones/zeros. In the RG/BA/SC, an all ones predictor achieves an average error of $44\% = 1 - (\text{average edge density})$. In the BAs, a naive all zeros predictor achieves $35\% = 1 - (\text{average edge density})$. This is useful to keep in mind when interpreting the results in Table 1.

Pseudo-synthetics. The Pseudo-Synthetic datasets are those in which we diffuse synthetic signals over SCs from the HCP-YA dataset. This is an ideal setting to test the GDN models: we have weighted graphs to perform edge-regression on (the others are unweighted), while having \mathbf{A}_O 's that are true to our modeling assumptions. Note that SCs have a strong community-like structure, corresponding dominantly to the left and right hemispheres as well as subnetworks which have a high degree of connection, e.g. the Occipital Lobe which has 0.96 edge density - almost fully connected - while the full brain network has edge density of 0.56.

Normalization. Unless otherwise stated we divide \mathbf{A}_O by its maximum eigenvalue before processing. \mathbf{A}_L is used in its raw form when it is an unweighted graph. The SCs define weighted graphs and we scale all edge weights to be between 0 and 1 by dividing by 9.9 (an upper bound on the maximum edge weight in the HCP-YA dataset). Similar to [32, 33], we find GLAD to be very sensitive to the conditioning of the labels \mathbf{A}_L ; see the Appendix A.8 for a full discussion on the normalization used in this case.

Error and MSE of the baselines in Table 1. The edge weights returned by the baselines can be very small/large in magnitude and perform poorly when used directly in the regression task. We thus also provide a learned scaling parameter, tuned during the hyperparameter search, which provides approximately an order of magnitude improvement in MSE in GLASSO and halved the MSE in Spectral Templates and Network Deconvolution. In link-prediction, we also tune a hard thresholding parameter on top of each method to clean up noisy outputs from the baseline, only if it improved their performance (it does). For complete details on the baseline implementation; see the Appendix A.8. Note also that the MSE reported in Table 1 is per-edge squared error - averaged over the test set, namely $\frac{1}{M} \frac{1}{|\mathcal{T}_{test}|} \sum_{i=1}^{|\mathcal{T}_{test}|} \|\Phi(\mathbf{A}_O^{(i)}) - \mathbf{A}_L^{(i)}\|_F^2$, where $M := N(N - 1)$ is the number of edges in a fully connected graph (without self loops) with $N = 68$ nodes.

Size generalization. Something to note is that we do **not** tune the threshold (found during training on the small $N = 68$ graphs) on the larger graphs. We go straight from training to testing on the larger domains. Tuning the threshold using a validation set (of larger graphs) would represent an easier problem. The model at no point, or in any way, is introduced to the data in the larger size domains for any form of training/tuning.

We decide to use the covariance matrix in this experiment, as opposed to the sample covariance matrix, as our \mathbf{A}_O 's. This is for the simple reason that it would be difficult to control the snr with respect to generalization error and would be secondary to the main thrust of the experiment. When run with number of signals proportional to graph size, we see quite a similar trend, but due to time constraints, these results are not presented herein, but is apt for follow up work.

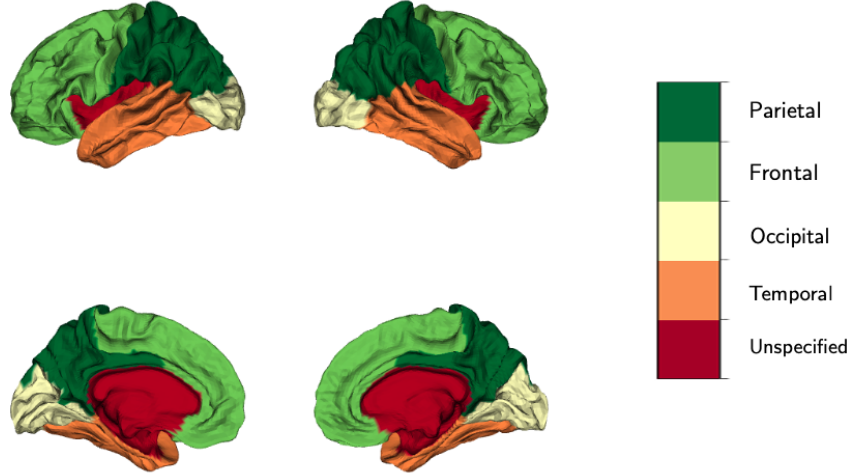


Figure 6: The four lobes in the brains cortex.

HCP data. HCP-YA provides up to 4 resting state fMRI scanning sessions for each subject, each lasting 15 minutes. We use the fMRI data which has been processed by the minimal processing pipeline [52]. For every subject, after pre-processing the time series data to be zero mean, we concatenate all available time-series together and compute the sample covariance matrix (which is what as used are \mathbf{A}_O in the brain data experiment 5.2).

Due to expected homogeneity in SCs across a healthy population, information about the SC in the test set could be leveraged from the SCs in the training set. In plainer terms, the average SC in the training set is an effective predictor of SCs in the test set. In our experiments, we take random split of the 1063 SCs into 913/50/100 training/validation/test sets, and report how much we improve upon this predictor.

In summary, our pseudo-synthetic experiments in Section 5.1 show that SCs are amenable to learning with GDNs when the SC-FC relationship satisfies (1), a reasonable model given the findings of [17]. In general, SC-FC coupling can vary widely across both the population and within the sub-regions of an individuals brain for healthy subjects and in pathological contexts. When trained on the HCP-YA dataset, GDNs exhibit robust performance over such regions with high variability in SC-FC coupling. Therefore, our results on HCP-YA dataset could potentially serve as baselines that characterize healthy subjects in pathology studies in future work, where the pathology could be characterized by specific deviations with respect to our results.

Raw data available from <https://www.humanconnectome.org/study/hcp-young-adult/overview>, and subject to the HCP Data Use Agreement. See here for a discussion on the risks of personal identifiability.

Co-location and social networks among high school students. The Thiers13 dataset [55] followed students in a French high school in 2013 for 5 days, recording their interactions based on physical proximity (co-location) using wearable sensors as well as investigating social networks between students via survey. The co-location study traced 327 students, while a subset of such students filled out the surveys (156). We thus only consider the 156 students who have participated in both studies. The co-location data is a sequence of time intervals, each interval lists which students were within a physical proximity to one another in such interval. To construct the co-location network, we let vertices represent students and assign the weight on an edge between student i and student j to represent the (possibly 0) number of times over the 5 day period the two such students were in close proximity with one another. The social network is the Facebook graph between students: vertex i and vertex j have an unweighted edge between them in the social network if student i and student j have are friends in Facebook. Thus we now have a co-location network $\mathbf{A}_{O,\text{total}}$ and a social network $\mathbf{A}_{L,\text{total}}$. To construct a dataset of graph pairs $\mathcal{T} = \{\mathbf{A}_O^{(i)}, \mathbf{A}_L^{(i)}\}_{i=1}^{7000}$ we draw random subsets of $N = 120$ vertices (students). For each vertex subset, we construct a single graph pair by restricting the vertex set in each network to the sampled vertices, and removing all edges which attach to any

node not in the subset. If either of the resulting graph pairs are not connected, the sample is not included.

The performance of the baselines are as follows: Threshold ($10.2 \pm 1.2e-2\%$), ND ($10.2 \pm 1.2e-2\%$), GLASSO (NA - could not converge for any of the α values tested), SpecTemps ($10.7 \pm 6.9e-2\%$), GLAD ($14.7 \pm 1.3e-2\%$). We report performance of each model with an additional tuned threshold on the output, only if it helps. ND does not change the output meaningfully (and thus the performance is identical to simply thresholding). GLAD continually converged to local minimum with worse performance than simple thresholding. Due to the scaling issues - and resulting large computational costs - a subset of this dataset is used for ND (train/val/test of 500/100/200) and GLASSO/SpecTemps (train/val/test of 20/20/85). Increasing dataset sizes further did not seem to improve performance for any model.

A.8 Baselines

In the broad context of network topology identification, recent latent graph inference approaches such as DGCNN [29], DGM [9], NRI [31], or PGN [30] have been shown effective in obtaining better task-driven representations of relational data for machine learning applications, or to learn interactions among coupled dynamical systems. However, because the proposed GDN layer does not operate over node features, none of these state-of-the-art methods are appropriate for tackling the novel network deconvolution problem we are dealing with here. Hence, for the numerical evaluation of GDNs we chose the most relevant baseline models that we outline in Section 5, and further describe in the sequel.

We were as fair as possible in the comparison of GDNs to baseline models. All baselines were optimized to minimize generalization error, which is what is presented in Table 1. Many baseline methods aim to predict sparse graphs on their own, yet many fail to bring edge values fully to zero. We thus provide a threshold, tuned for generalization error using a validation set, on top of each method only if it improved the performance of the method in link-prediction. The edge weights returned by the baselines can be very small/large in magnitude and perform poorly when used directly in the regression task. We thus also provide a scaling parameter, tuned during the hyperparameter search, which provides approximately an order of magnitude improvement in MSE for GLASSO and halved the MSE for Spectral Templates and Network Deconvolution.

Hard Thresholding (Threshold). The hard thresholding model consists of a single parameter τ , and generates graph predictions as follows

$$\hat{A}_L = \mathbb{I}\{|A_O| \succeq \tau \mathbf{1}\mathbf{1}^\top\},$$

where $\mathbb{I}\{\cdot\}$ is an indicator function, and \succeq denotes entry-wise inequality. For the synthetic experiments carried out in Section 5.1 to learn the structure of signals generated via network diffusion, A_O is either a covariance matrix or a correlation matrix. We tried both choices in our experiments, and reported the one that performed best in Table 1.

Graphical Lasso (GLASSO). GLASSO is an approach for Gaussian graphical model selection [56, 21]. In the context of the first application domain in Section 3, we will henceforth assume a zero-mean graph signal $x \sim \mathcal{N}(\mathbf{0}, \Sigma_x)$. The goal is to estimate (conditional independence) graph structure encoded in the entries of the precision matrix $\Theta_x = \Sigma_x^{-1}$. To this end, given an empirical covariance matrix $A_O := \hat{\Sigma}_x$ estimated from observed signal realizations, GLASSO regularizes the maximum-likelihood estimator of Θ_x with the sparsity-promoting ℓ_1 norm, yielding the convex problem

$$\hat{\Theta} \in \arg \max_{\Theta \succeq 0} \left\{ \log \det \Theta - \text{trace}(\hat{\Sigma}_x \Theta) - \alpha \|\Theta\|_1 \right\}. \quad (8)$$

We found that taking the entry-wise absolute value of the GLASSO estimator improved its performance, and so we include that in the model before passing it through a hard-thresholding operator

$$\hat{A}_L = \mathbb{I}\{|\hat{\Theta}| \succeq \tau \mathbf{1}\mathbf{1}^\top\}$$

One has to tune the hyperparameters α and τ for link-prediction (and a third, the scaling parameter described below, for edge-weight regression).

We used the sklearn GLASSO implementation found here: https://scikit-learn.org/stable/modules/generated/sklearn.covariance.graphical_lasso.html

It is important to note that we do **not** use the typical cross-validation procedure seen with GLASSO. Typically, GLASSO is used in unsupervised applications with only one graph being predicted from s observations. In our application, we are predicting many graphs, *each* with s observations. Thus the typical procedure of choosing α using the log-likelihood [the non-regularized part of the GLASSO objective in (8)] *over splits of the observed signals, not splits of the training set*, results in worse performance (and a different α for each graph). This is not surprising: exposing the training procedure to labeled data allows it to optimize for generalization. We are judging the models on their ability to generalize to unseen graphs, and thus the typical procedure would provide an unfair advantage to our model. While we tried both sample covariance and sample correlation matrices as \mathbf{A}_O , we found that we needed the normalization that the sample correlation provides, along with an additional scaling by the maximum magnitude eigenvalue, in order to achieve numerical stability. GLASSO can take a good amount of time to run, and so we limited the validation and test set sizes to an even 100/100 split. With only 2 to 3 hyperparameters to tune, we found this was sufficient (no significant differences between validation and test performance in all runs, and when testing on larger graph sizes, no difference in generalization performance).

Unrolled AM on GLASSO Objective (GLAD) GLAD is an unrolling of an Alternating Minimization (AM) iterative procedure to solve the Gaussian model selection problem discussed above (8); refer to [32] for full details. GLAD inherits sensitivity to the conditioning of the labels from the constraint that Θ be positive semi-definite in (8). In the experiments presented in [32], precision matrices are sampled directly to be used as labels, and their minimum eigenvalue is set to 1.0 by adding an appropriately scaled identity matrix. This minimum eigenvalue correction was attempted on the raw adjacency matrices \mathbf{A}_L but did not result in convergent training on any data domain in our experiments. The best results (reported in Table 1) were found corresponding to the minimum eigenvalue corrected Laplacian matrix representation of the latent graph - $\mathbf{L}_L := \text{diag}(\mathbf{A}_L \mathbf{1}) - \mathbf{A}_L + \mathbf{I}$. \mathbf{L}_L - referred to as Θ^* in [32] - is used *only in the the loss function* to make training converge. The reported metrics in Table 1 disregard the diagonal elements and compute error and mse based on the off-diagonal entries, thus ensuring an equivalent comparison with all other methods. Finally, for the link-prediction task, a threshold τ is chosen with a validation set to map the output to binary decision over edges in the same manner as used in GDNs - see A.4.

We use the GLAD configuration as presented in [32]: $L = 30$ layers, adam optimizer with learning rate $lr = .1$ and $\beta_1 = .9, \beta_2 = .999$, the ρ_{nn} has 4 hidden layers, and Λ_{nn} has 2 hidden layers. An intermediate loss discount factor $\gamma = 0.8$ worked reasonably well in the domains tested. *ER* graphs caused GLAD to converge to a trivial all zeros solution when $D = 30$. We increased the depth to $D = 50$ and performed a search over the learning rate and minimum eigenvalue m_e (previously set to 1), resulting in a GLAD model ($D = 50, lr = .05, m_e = 100$, all other identical) that decreased error (by 1%) in the link-prediction task relative to the naive all zero output. MSE got worse in this configuration relative to the previous. In Table 1 we report respective metrics from their best configurations: the error with the deeper configuration and *MSE* with the shallower configuration.

When training on the SCs in Table 1, we incorporate prior information in GLAD by setting the prior to $\text{diag}(\mathbf{A}\mathbf{1}) - \mathbf{A} + \mathbf{I}$, where \mathbf{A} is the adjacency matrix of the edgewise mean graph over all SCs in the training split. In other words we use the minimum eigenvalue corrected Laplacian matrix (as above) representation of \mathbf{A} . GDNs simply use \mathbf{A} as discussed in Section 5. We also tried the default setup, where the prior is $(\mathbf{A}_O + \mathbf{I})^{-1}$, but found inferior performance.

GLAD in general has an $\mathcal{O}(DN^3)$ run time complexity, where D is the depth of GLAD, in both the forward and the backward pass, due to the computation of the matrix square root and its corresponding gradient. These can be approximated using e.g. Denman-Beavers iterations or Newton-Schulz iterations, which reduce the time complexity to $\mathcal{O}(DTN^2)$, where T is the number of iterations run. These iterative methods still lack guarantees of convergence in general. We used such approximations without noticing reductions in performance to make the experiments run in reasonable amounts of time. Even with such approximations GLAD has significant memory and runtime limitations. This results from the large D , moderate sized T (required for reasonable/stable approximations), as well as the use of shared intermediate MLPs - ρ_{nn} and Λ_{nn} - the former of which is called N^2 times (one for each entry in Θ) *per layer*. This forces batch sizes smaller than what would be desired and limits applicability on larger graph sizes. Note that in contrast the dominant term in the memory & time complexity of GDN layers are the 2 (typically sparse) matrix multiplications, making training and deployment on larger graph sizes realizable; see Figure 3.

Network Deconvolution (ND). The Network Deconvolution approach is “a general method for inferring direct effects from an observed correlation matrix containing both direct and indirect effects” [8]. Network Deconvolution follows three steps: linear scaling to ensure all eigenvalues λ_i of \mathbf{A}_O fall in the interval $\lambda_i \in [-1, 1]$, eigen-decomposition of the scaled $\mathbf{A}_O = \mathbf{V} \text{diag}(\boldsymbol{\lambda}) \mathbf{V}^{-1}$, and deconvolution by applying $f(\lambda_i) = \frac{\lambda_i}{1+\lambda_i}$ to all eigenvalues. We then construct our prediction as $\hat{\mathbf{A}}_L := \mathbf{V} \text{diag}(f(\boldsymbol{\lambda})) \mathbf{V}^{-1}$. In [8], it is recommended a Pearson correlation matrix be constructed, which we followed. We applied an extra hard thresholding on the output, tuned for best generalization error, to further increase performance. For each result shown 500 graphs were used in the hyperparameter search and 500 were used for testing.

Spectral Templates (SpecTemp). The SpecTemp method consists of a two-step process whereby one: (i) first leverages the model (1) to estimate the graph eigenvectors \mathbf{V} from those of \mathbf{A}_O (the eigenvectors of \mathbf{A}_L and \mathbf{A}_O coincide); and (ii) combine \mathbf{V} with a priori information about G (here sparsity) and feasibility constraints on \mathcal{A} to obtain the optimal eigenvalues $\boldsymbol{\lambda}$ of $\mathbf{A}_L = \mathbf{V} \text{diag}(\boldsymbol{\lambda}) \mathbf{V}^\top$.

The second step entails solving the convex optimization problem

$$\begin{aligned} \mathbf{A}^*(\epsilon) := & \underset{\{\mathbf{A}, \bar{\boldsymbol{\lambda}}\}}{\text{argmin}} \|\mathbf{A}\|_1, & (9) \\ \text{s. to } & \|\mathbf{A} - \mathbf{V} \text{diag}(\bar{\boldsymbol{\lambda}}) \mathbf{V}^\top\|_2^2 < \epsilon, \mathbf{A} \succeq \mathbf{1}, \mathbf{S} \in \mathcal{A}. \end{aligned}$$

We first perform a binary search on $\epsilon \in \mathbb{R}_+$ over the interval $[0, 2]$ to find ϵ_{min} , which is the smallest value which allows a feasible solution to (9). With ϵ_{min} in hand, we now run an iteratively (t henceforth denotes iterations) re-weighted ℓ_1 -norm minimization problem with the aim of further pushing small edge weights to 0 (thus refining the graph estimate). Defining the weight matrix $\mathbf{W}_t := \frac{\gamma \mathbf{1}\mathbf{1}^\top}{|\mathbf{A}_{t-1}^*| + \delta \mathbf{1}\mathbf{1}^\top} \in \mathbb{R}_+^{N \times N}$ where $\gamma, \delta \in \mathbb{R}_+$ are appropriately chosen positive constants and $\mathbf{A}_0^* := \mathbf{A}^*(\epsilon_{min})$, we solve a sequence $t = 1, \dots, T$ of weighted ℓ_1 -norm minimization problems

$$\begin{aligned} \mathbf{A}_t^* := & \underset{\{\mathbf{A}, \bar{\boldsymbol{\lambda}}\}}{\text{argmin}} \|\mathbf{W}_t \odot \mathbf{A}\|_1, & (10) \\ \text{s. to } & \|\mathbf{A} - \mathbf{V} \text{diag}(\bar{\boldsymbol{\lambda}}) \mathbf{V}^\top\|_2^2 < \epsilon_{min}, \mathbf{A} \succeq \mathbf{1}, \mathbf{A} \in \mathcal{A}. \end{aligned}$$

If any of these problems is infeasible, then \mathbf{A}_I^* is returned where $I \in \{0, 1, \dots, T\}$ is the last successfully obtained solution.

Finally, a threshold τ is chosen with a validation set to map the output to binary decision over edges, namely

$$\hat{\mathbf{A}}_L = \mathbb{I} \{ |\mathbf{A}_I^*| \succeq \tau \mathbf{1}\mathbf{1}^\top \},$$

We solve the aforementioned optimization problems using MOSEK solvers in CVXPY. Solving such convex optimization problems can very computationally expensive/slow, and because there are only two hyperparameters, 100 graphs were used in the validation set, and 100 in the test set.

Least Squares plus Non-convex Optimization (LSOpt). LSOpt consists of first estimating the polynomial coefficients in (1) via least-squares (LS) regression, and then using the found coefficients in the optimization of (3) to recover the graph \mathbf{A}_L . Due to the collinearity between higher order matrix powers, ridge regression can be used in the estimation of the polynomial coefficients. If the true order K of the polynomial is not known ahead of time, one can allow $\hat{\mathbf{h}} \in \mathbb{R}^N$ and add an additional ℓ_1 -norm regularization for the sake of model-order selection. With $\hat{\mathbf{h}}$ in hand, we optimize (3), a non-convex problem due to the higher order powers of \mathbf{A} , using Adam with a learning rate of 0.01 and a validation set of size 50 to tune λ .

We start with the most favorable setup, using the true \mathbf{h} in the optimization of (3), skipping the LS estimation step. Even in such a favorable setup the results were not in general competitive with GDN predictions, and so instead of further degrading performance by estimating $\hat{\mathbf{h}}$, we report these optimistic estimates of generalization error.

A.9 Source Code and Configuration

Code has been made available in a zipped directory with the submission. We rely on PyTorch [57] (BSD license) heavily and use Conda [58] (BSD license) to make our system as hardware-independent as possible. GPUs were used to train the larger GDNs, which are available to use for free

on Google Colab. Development was done on Mac and Linux (Ubuntu) systems, and not tested on Windows machines. The processed brain data was too large to include with the code, but is available upon request.